Cluster formation by acoustic forces and active fluctuations in levitated granular matter

Melody X. Lim,[1,2] Anton Souslov,[1,3] Vincenzo Vitelli,[1,2] and Heinrich M. Jaeger[1,2]

[1] *James Franck Institute, The University of Chicago, Chicago, Illinois 60637, USA*
[2] *Department of Physics, The University of Chicago, Chicago, Illinois 60637, USA*
[3] *Department of Physics, University of Bath, Bath BA2 7AY, United Kingdom*

Mechanically agitated granular matter often serves as a prototype for exploring the rich physics associated with hard sphere systems, with an effective temperature introduced by vibrating or shaking [1–6]. While depletion interactions drive clustering and assembly in colloids [7–10], no equivalent short-range attractions exist between macroscopic grains. Here we overcome this limitation and investigate granular cluster formation by using acoustic levitation and trapping [11–13]. Scattered sound establishes short-range attractions between small particles [14], while detuning the acoustic trap generates active fluctuations [15]. To illuminate the interplay between attractions and fluctuations, we investigate transitions among ground states of two-dimensional clusters composed of a few particles. Our main results, obtained using experiments and modelling, reveal that, in contrast to thermal colloids, in non-equilibrium granular ensembles the magnitude of active fluctuations controls not only the assembly rates but also their assembly pathways and ground-state statistics. These results open up new possibilities for non-invasively manipulating macroscopic particles, tuning their interactions, and directing their assembly.

In two dimensions, particle clusters with five or fewer constituents have only one compact configuration, i.e., one isostatic ground state [16] (Fig. 1a). However, beginning with six particles, there are an increasing number of energetically degenerate, but geometrically distinct, ground-state configurations. This complex energy landscape has been studied with colloids in thermal equilibrium [9, 16]. Here, we explore the ground-state statistics in ensembles of macroscopic particles driven by active fluctuations that emerge from the dynamics of a driven system rather than from coupling to a heat bath. We demonstrate how energetic degeneracies, assembly rates, and pathways are altered during out-of-equilibrium assembly.

To eliminate frictional interactions with container walls we levitate particles in a sound pressure field. The same field also induces short-range, tunable nonlinear attractions that we here call acoustic forces. Not unlike depletion forces in colloids [18] or other Casimir-like forces, these acoustically-mediated attractions can generate robust particle clusters. This differs from the formation of clusters in granular media due to external confinement [1, 19] or, transiently, due to inelastic collisions [1, 19–21]. Furthermore, the acoustic forces scale with the sound pressure amplitude, which enables precise control over cluster energetics. Such control provides advantages over cohesive forces due to capillary bridges, van der Waals interactions, or charging [22, 23]. Finally, in contrast to induced electric or magnetic dipole forces [24], the acoustic interactions are not aligned with an applied vector field and, due to nonlinearity, acoustic forces depend on particle motion [25].

Our setup is illustrated in Fig. 1b. We generate a standing wave of the acoustic pressure field between an ultrasound transducer and the (transparent) acrylic reflector. Polyethylene particles (diameter 710-850μm) levitate within a horizontal plane one-quarter of the gap height from the reflector. We image these acoustically trapped particles from the side (Fig. 1c), or from below (Fig. 1d) using a high-speed camera. When multiple particles are placed in the trap, they form compact clusters. Images of the resulting configurations for six- and seven-particle clusters are shown in Fig. 1d. Six-particle systems have three distinct ground-state configurations: parallelogram (P), chevron (C), and triangle (T). For 7-particle clusters, there are four distinct topologies: Flower (Fl), Tree (Tr), Turtle (Tu), and Boat (Bo).

Whereas colloidal clusters can be stabilised by depletion forces, acoustically levitated clusters are stabilised by in-plane acoustic forces, which are short-range pairwise [12, 26] attractions generated by acoustic scattering. At close approach, these Casimir-like forces F between spherical particles scale as

$$F \sim \frac{E_0 a^6 \lambda^{-3}}{r^4} \tag{1}$$

where $E_0 \equiv \rho_0 v_0^2/2$ is the energy density of the sound field having amplitude v_0 and wavelength λ in air (density ρ_0) [17]. The particles have radius a (which enters Eq. (1) with a sixth power) and are distance r ($\ll \lambda$) apart. For arbitrary separation, these forces can be approximated analytically [17], or calculated in more detail with finite-element simulations using either the Gor'kov approximation [11] or fluid-structure interactions [27] (see Methods and Supplementary Information). These calculations, shown in Fig. 1e, indicate that cluster energetics are dominated by the strong short-range ($r \lesssim 0.3\lambda$) attractions between nearest neighbours, as captured in Eq. (1). In addition, due to the finite lateral extent of the transducer, the levitation potential exhibits a small radial gradient. However, near the center of the trap this effect is negligibly small compared to the acoustic forces

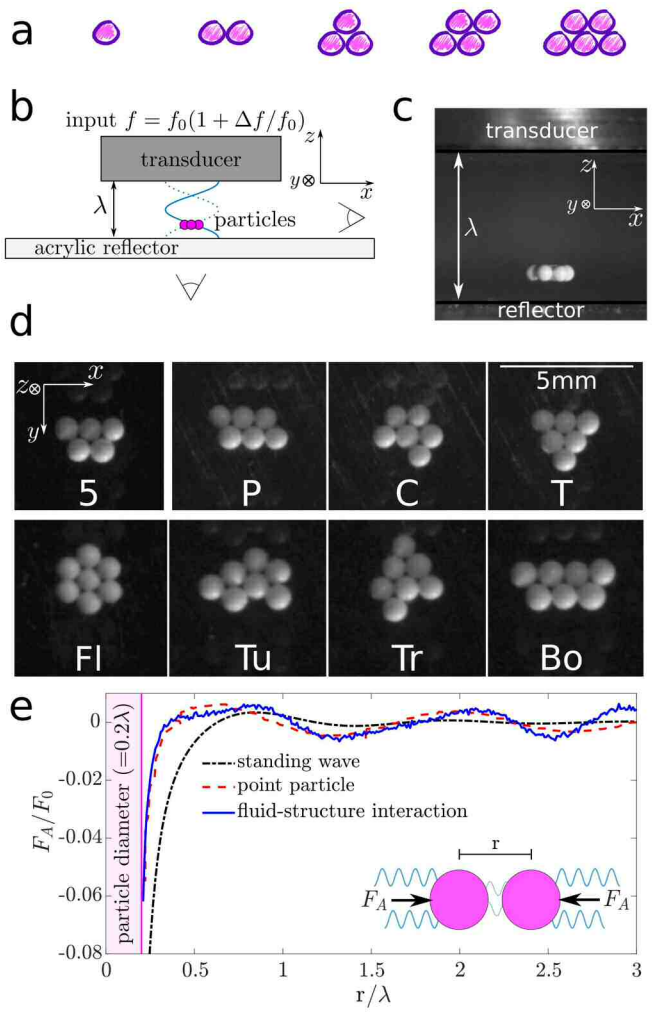

FIG. 1. **Assembling and manipulating clusters composed of macroscopic particles using acoustic levitation.** (a) Sketches of compact cluster configurations (isostatic ground states) for one to five particles. (b) Schematic of experimental setup. An ultrasound transducer generates sound waves in air, with speed of sound $c_s = 343$m/s. The distance between transducer and transparent acrylic reflector is chosen to create a pressure standing wave (blue line) with two nodes, at frequency $f_0 = 45.65$kHz and wavelength c_s/f_0. Polyethylene particles are acoustically levitated in the lower of the two nodes. Clusters are imaged from the side (b), as well as from below via a mirror (c). (d) Different cluster configurations, imaged from below. (Top) In two dimensions, there is only one 5-particle cluster configuration, but six particles can form one of three distinct ground states: parallelogram P, chevron C, and triangle T. (Bottom) Seven-particle clusters have four compact configurations: flower Fl, turtle Tu, tree Tr, and boat Bo. (e) The scattering of the acoustic field generates short-range attractions (secondary acoustic forces) within the levitation plane, which stabilise particle clusters. Force between two particles as a function of distance r between their centres, normalised by the particle weight $F_0 \equiv m_0 g$. Finite-element simulations (red dashed, blue solid lines) are compared to an analytical solution for particles in a vertical standing wave of infinite lateral extent [17] (black dashed-dotted line). See Methods and Supplementary Information for details, and SI Fig. S4 for a comparison to the primary force from the confining acoustic field in a trap of finite lateral extent. (Inset) Schematic illustrating the secondary acoustic force due to scattering between two particles in an acoustic field.

which stabilise the clusters (see Supplementary Information).

The acoustic trap can also induce non-conservative forces. Specifically, we use the fact that the particle dynamics in the acoustic field are underdamped (in contrast to colloids in a liquid) to drive instabilities that generate active fluctuations. As Ref. [15] shows, a sound wave with frequency f tuned just slightly larger than the standing wave resonance condition acts on a levitated object with a destabilising force proportional to the object's speed. [This force depends on the frequency f, which does not enter Eq. (1).] As a result, the clusters fluctuate up and down in the trap, occasionally hitting the reflector. This impact transfers kinetic energy from center-of-mass motion to modes that bend the cluster out of its planar, two-dimensional configuration. For sufficiently high amplitudes, these active fluctuations can lead to rearrangements between the different ground states (see Supplementary Movies 1 & 2). Finite-element simulations show that the detuning affects the magnitude of the attractive force between particles by less than 10% (see SI Fig. S3 for details).

Close to resonance, 6-particle clusters rearrange by ejecting a single particle, which then travels many particle diameters in a curved trajectory before it re-joins the 5-particle cluster from a random angle of approach. Once the particle re-joins, it becomes stuck due to the short-range attraction. This sticky, far-from-equilibrium assembly pathway is shown in Fig. 2a. The corresponding cluster statistics retain memory of the formation process [12]: the ground-state configuration is determined by the spatial angle of approach that the sixth particle takes towards the 5-particle cluster (see Supplementary Movie 3). Assuming that docking onto the 5-cluster is equally likely for any angle of approach (see Fig. 2a), the probabilities of forming P, C, or T 6-clusters are 1/2, 1/3, and 1/6, respectively, in close agreement with the data for the sticky limit (Fig. 2b).

By contrast, deep into the off-resonant regime, clusters rearrange by moving particles randomly along their periphery (Fig. 2c). This occurs either by single particle ejection with much shorter trajectories (i.e., no more than one particle diameter) or by 'floppy' hinge motions: When all but one of the bonds to nearest neighbours is broken by active cluster fluctuations, the remaining bond acts as a flexible hinge. This enables the particle to swing around to a new position without leaving the cluster. In this off-resonant regime, we find that P and C clusters occur with equal probability and twice as often as T clusters (Fig. 2b). Such cluster statistics correspond to an unbiased sampling of configuration space, where we simply count the number of ways a 6-cluster can be formed by adding one more particle to a 5-cluster. This ergodic limit is indistinguishable from the thermal case, which Ref. [16] observed using 6-particle clusters composed of micrometre-sized Brownian colloids.

By changing the ultrasound frequency, we can control the amplitude of active fluctuations and thus control the

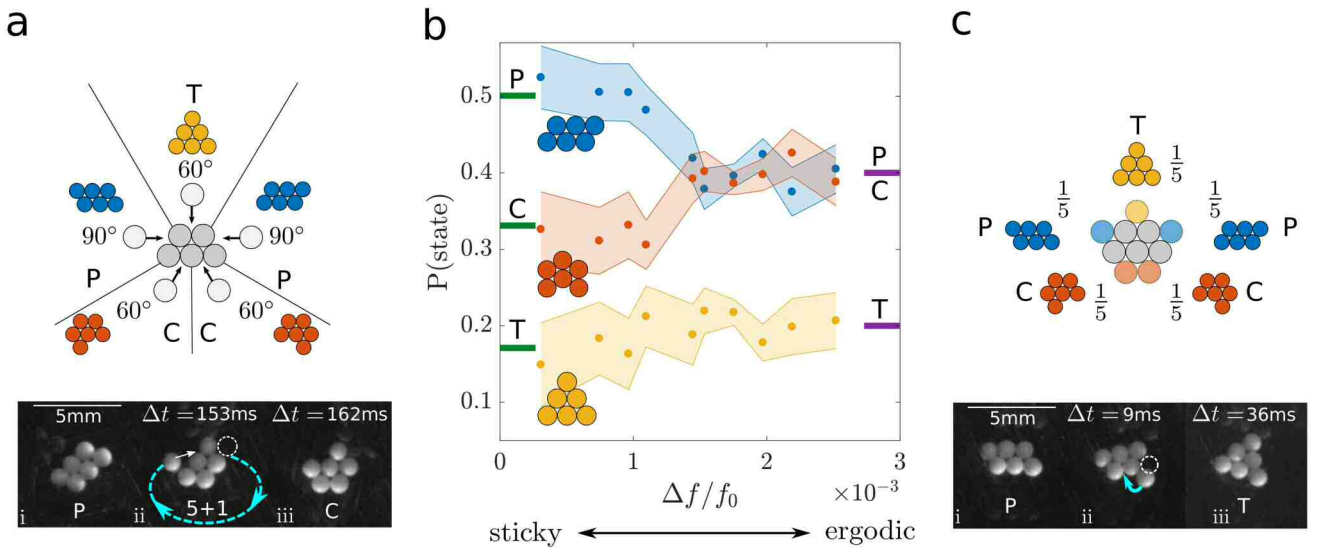

FIG. 2. **Tuning 6-particle assembly between sticky and ergodic limits.** Near resonance, cluster statistics follow sticky assembly (a). As the acoustic trap is detuned by increasing the sound frequency (b), cluster statistics change to ergodic assembly (c). (a) Model of sticky assembly: In the regime of small detuning parameter, $\Delta f/f_0 > 0$, the likelihood of a cluster configuration is determined by the geometric angle of approach of a sixth particle to the 5-particle cluster (top). (Bottom) Sequence of images from below showing a sticky rearrangement pathway. See Supplementary Movies 1 and 3 for dynamics. (b) Steady-state probabilities for 6-particle-cluster ground-state configurations as a function of detuning parameter. Note that the extremes of low and high detuning parameter are well captured by the predictions of physical models from parts (a) and (c), respectively. Standard error is indicated by shaded region. Horizontal bars indicate model predictions for the sticky and ergodic limits (see text). (c) Model of ergodic assembly: For larger detuning, the sixth particle has equal probability of occupying each of the five binding sites on the five-particle cluster (top). (Bottom) Sequence of images from below showing a transition between ground states in the ergodic regime through a hinge motion. See Supplementary Movies 1 and 4 for dynamics, and Supplementary Information for the number of observations in this data.

cluster rearrangement processes. Figure 2b shows statistics for relative ground-state probabilities as a function of detuning parameter $\Delta f/f_0$, where f_0 (= 45.65kHz) is the trap resonant frequency, f is the driving frequency, and $\Delta f \equiv f - f_0 > 0$. As the trap is detuned, cluster statistics transition smoothly from sticky to ergodic. At the same time, clusters increasingly rearrange via hinge motions (see Supplementary Movie 4).

The emergence of hinge motions is closely linked to out-of-plane bending, which like particle ejection is triggered by impacts against the reflector, as shown in Fig. 3a (see also Supplementary Movie 2). We quantify the associated deviation from planar configuration by computing the second moment J of the vertical pixel coordinates z associated with a cluster in side-view (see Methods). For a fully planar configuration, J is at a minimum; if the cluster is bent out of plane, J increases. Representative time series of J for small and large detuning parameters are shown in Fig. 3a. From longer versions of such time series, the probability distributions $P(J)$ for finding a particular magnitude J can be extracted. As Fig. 3b shows, clusters remain effectively rigid and planar for small $\Delta f/f_0$, while further detuning generates a rapidly increasing probability of exciting large-J values associated with shape-changing, out-of-plane bending fluctuations. These fluctuations also become more frequent (Fig. 3a, bottom), resulting in broad power spectra whose magnitude quickly rises with $\Delta f/f_0$, while their overall character changes little (Fig. 3c).

When we plot the average power per octave (i.e. the average total power in the frequency interval from frequency f_1 to frequency $2f_1$) associated with shape-changing fluctuations we find it to increase exponentially with detuning parameter $\Delta f/f_0$ (Fig. 3d). At the same time, we find that also the probability P_t of observing a transition between any two 6-particle ground states increases exponentially (Fig. 3e). Together, this shows that $\Delta f/f_0$ plays a role reminiscent of an effective temperature in an activated process: detuning the trap generates instabilities that temporarily break particle-particle bonds and allow for cluster rearrangement.

Here, a surprising aspect is that detuning not only controls the rate, but also the type of rearrangement process. From Fig. 2b, we see that these processes have important consequences for the likelihood of observing specific ground state configurations. In particular, the degeneracy between parallelogram (P) and chevron (C) in the ergodic limit can be broken by moving to the regime dominated by sticky assembly.

Driven by active fluctuations, these clusters explore an athermal ensemble. The cluster reconfigurations are instances of a general transition process through interme-

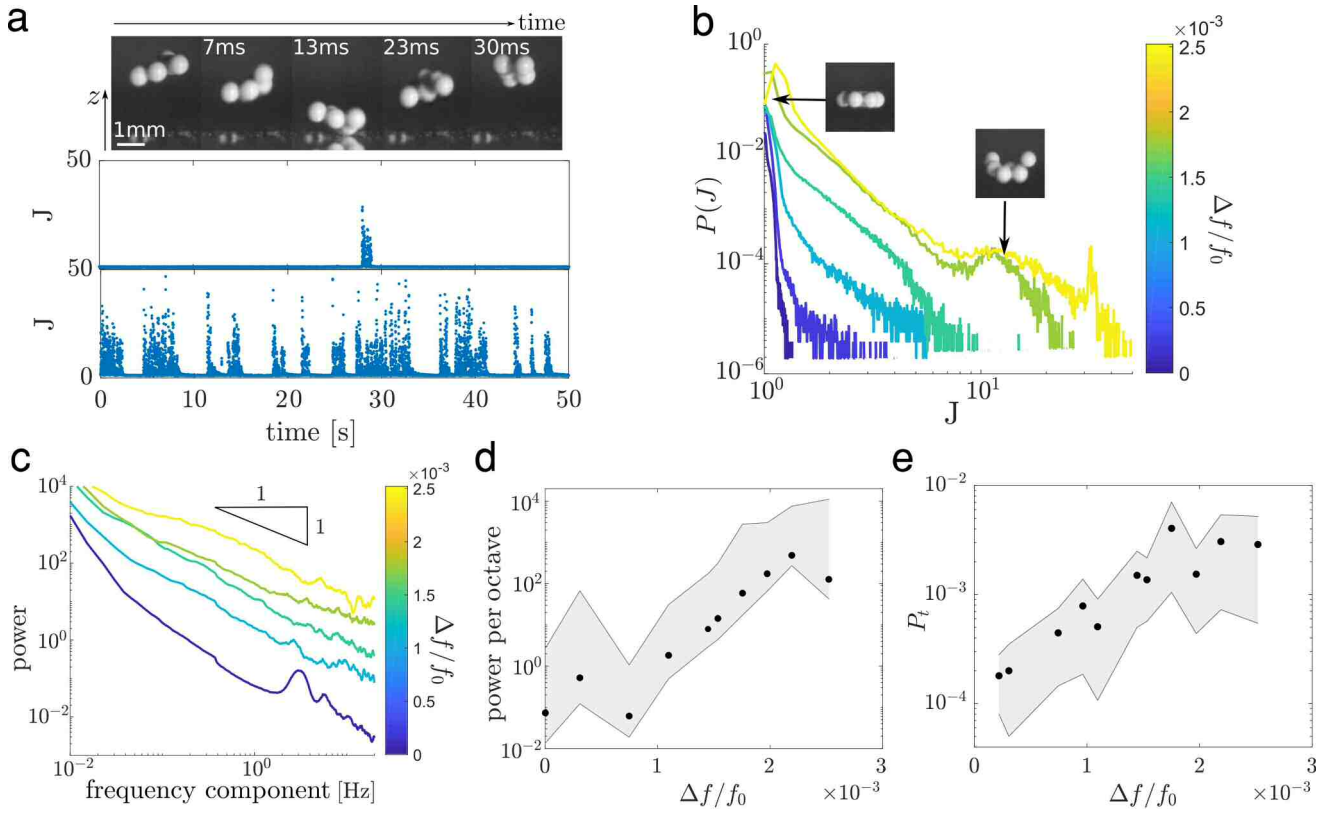

FIG. 3. **Out-of-plane motion as a measure of active fluctuations.** (a) (Top) Sequence of side images showing a cluster colliding with the reflector. See Supplementary Movie 2 for dynamics. Time series for second moment J of vertical coordinate z (see Methods), for small detuning (middle) and large detuning (bottom). (b) Probability distribution of J as function of detuning parameter, obtained from time series as in part (a). Illustrative side images of clusters are shown at their value of J. (c) Power spectrum of the J time series. (d) Average power per octave as function of detuning parameter. (e) P_t, the probability of transition between any cluster ground state, as a function of detuning parameter. Shaded areas in (d) and (e) indicate the standard error. Note the similar trends in (d) and (e): the fluctuations increase exponentially as the system is detuned away from resonance.

diate states. We model this process with a discrete-time Markov chain, in which state transition matrices represent the creation of specific ground state configurations through adding or removing one particle. To represent the various ground-state probabilities P_i for a general N-particle cluster, we list them as i components of a vector $\mathbf{P}_N$. Specifically for $N = 6$, $\mathbf{P}_6 = (P_P, P_C, P_T)$, where the subscripts refer to the three possible configurations. The (i, j)-th element of the transition matrix T_N represents the probability of creating the i-th N-particle ground state by adding a single particle to the j-th $(N-1)$-particle ground state. Similarly, the (i, j)-th element of the matrix Q_N captures how the i-th N-particle state is obtained by destroying the j-th ground state of the $(N+1)$-particle cluster. Under steady-state conditions, $\mathbf{P}_N$ is related to the probabilities $\mathbf{P}_{N-1}$ and $\mathbf{P}_{N+1}$ through

$$\mathbf{P}_N = \mathrm{T}_N \mathbf{P}_{N-1} + \mathrm{Q}_N \mathbf{P}_{N+1} \,. \qquad (2)$$

Once T_N and Q_N are known, Eq. (2) can be solved recursively for $\mathbf{P}_N$ (see Methods). For the case discussed so far, with six particles in the trap, Eq. (2) leads to $\mathbf{P}_6 = \mathrm{T}_6 \mathbf{P}_5$ and $\mathbf{P}_5 = \mathrm{Q}_5 \mathbf{P}_6$, which gives $\mathbf{P}_6 = \mathrm{T}_6 \mathrm{Q}_5 \mathbf{P}_6$. Since removing any particle from a 6-cluster results in the same 5-cluster (so that $\mathbf{P}_5 = 1$), we have $\mathrm{Q}_5 = \begin{pmatrix} 1 & 1 & 1 \end{pmatrix}$. However, the 3×1 matrix T_6 depends on whether the creation process is sticky or ergodic, i.e., its components are the docking probabilities indicated in the top panels of Fig. 2a, c. Solving for $\mathbf{P}_6$ then gives the values indicated by the horizontal bars along either side of Fig. 2b, in close agreement with the data.

Having obtained T_6 and Q_5, we can now make predictions for the case that there are seven particles in the trap and $\mathbf{P}_7$ represents the four ground states shown in Fig. 1d. Figure 4a shows the reconfiguration pathways for 7-particle clusters and, as examples, transitions from boat to tree via hinge-motion and from flower to turtle via particle ejection and recapture. In the model, we assume that T_7 contains only processes that generate 7-from 6-particle states in an ergodic fashion. As a result, T_7 is a 4×3 matrix with elements corresponding to docking one particle at any available 6-cluster site with equal

probability (Fig. 4a).

Recursively solving Eq. (2) for $\mathbf{P}_7$, we find steady-state probabilities near 0.075, 0.47, 0.30 and 0.15 for the flower (Fl), tree (Tr), turtle (Tu) and boat (Bo) configurations (see Methods for details, and Supplementary Information for comparison to thermal 7-particle clusters). Importantly, the model indicates that all four 7-particle ground states should be largely insensitive to whether the 6-particle intermediate states are formed from 5-particle precursors via a sticky or ergodic process. These numerical values are in excellent agreement with the data (Fig. 4b).

A further model prediction concerns the probabilities for the intermediate 6-particle states in the 7-particle system, shown in Fig. 4c. As before, these states are strongly affected by whether the sticky or ergodic assembly process is followed. However, the probabilities differ from those for the ground states in the 6-particle system (Fig. 2b), since now T_7 and Q_6 enter the Markov-chain model. Again we find that these probabilities are consistent with the data.

This match between model and experiments justifies, *a posteriori*, the above assumption about the applicability of the ergodic form of T_7 across the whole range of $\Delta f/f_0$. However, we can also check this assumption directly. This is done in Fig. 4d, where we plot the experimentally observed probability of reconfiguration via hinge motion P_H relative to P_T as a function of the detuning parameter $\Delta f/f_0$. While for 6-clusters this fraction increases steadily with detuning, for 7-clusters it is effectively independent of $\Delta f/f_0$, just as the 7-cluster statistics. This difference in hinge-mode proliferation reflects that larger clusters support more bending modes and generate larger out-of-plane bending amplitudes along their periphery. We conclude that hinge motions serve as a key indicator for processes that generate ergodic reconfigurations among the ground states.

In this paper we used acoustic levitation to explore the formation and reconfiguration of small clusters of particles. While thermal fluctuations set the magnitude of depletion forces in more microscopic particle systems such as colloids, active fluctuations in the acoustic trap depend sensitively on the sound frequency. At the same time, the acoustic forces are not particularly sensitive to the sound frequency (see SI Fig. S2). This allows for the control of fluctuations independently from the interactions. The cluster statistics, in turn, emerge from the dynamic response of the levitated objects to detuning the acoustic trap.

We can envision acoustic levitation as a more general platform for non-invasive manipulation of granular matter with tunable attractive interactions and further exploration of nonequilibrium assembly. Our results open up new opportunities for investigating in the underdamped regime the dynamics of extended, 2D rafts of close-packed particles [28]. Since the levitated particles are macroscopic, anisotropy in acoustic forces could be achieved via particle shape and/or by combining materials with different sound scattering properties, as demonstrated by [29]. This may provide a means to assemble complex structures similar to what has been done with patchy colloids [10, 30] or shape-dependent entropic forces [31]. Longer-range interactions analogous to those between particles at curved fluid interfaces [32] could be implemented using the back-action of levitated grains on the sound field itself.

Acknowledgments We thank E. Klein and the Manoharan group for naming the seven-particle cluster configurations. We thank S. Waitukaitis, N. Schade, T. Witten, S. Nagel and R. Behringer for insightful discussions, and J. Z. Kim for a critical reading of the manuscript. This work is dedicated to the memory of R. Behringer. The research was supported by the National Science Foundation through grants DMR-1309611 and DMR-1810390. A.S. and V. V. acknowledge primary support through the Chicago MRSEC, funded by the NSF through grant DMR-1420709.

Author Contributions M.X.L. and H.M.J. conceived of the project and designed the experiments. M.X.L. performed the experiments and analysed the data. M.X.L and A.S. calculated the acoustic forces. M.X.L., A.S. and V.V. developed the model and performed the theoretical analysis. All authors contributed to writing the manuscript.

[1] Olafsen, J. & Urbach, J. Clustering, order, and collapse in a driven granular monolayer. *Physical Review Letters* **81**, 4369–4372 (1998).

[2] D'Anna, G., Mayor, P., Barrat, A., Loreto, V. & Nori, F. Observing brownian motion in vibration-fluidized granular matter. *Nature* **424**, 909–912 (2003).

[3] Feitosa, K. & Menon, N. Fluidized granular medium as an instance of the fluctuation theorem. *Physical Review Letters* **92**, 164301 (2004).

[4] Keys, A. S., Abate, A. R., Glotzer, S. C. & Durian, D. J. Measurement of growing dynamical length scales and prediction of the jamming transition in a granular material. *Nature Physics* **3**, 260–264 (2007).

[5] Komatsu, Y. & Tanaka, H. Roles of energy dissipation in a liquid-solid transition of out-of-equilibrium systems. *Physical Review X* **5**, 031025 (2015).

[6] Workamp, M., Ramirez, G., Daniels, K. E. & Dijksman, J. Symmetry-reversals in chiral active matter. *Soft Matter* **14**, 5572–5580 (2018).

[7] Manoharan, V. N., Elsesser, M. T. & Pine, D. J. Dense packing and symmetry in small clusters of microspheres. *Science* **301**, 483–487 (2003).

[8] Sacanna, S., Irvine, W. T. M., Chaikin, P. M. & Pine, D. J. Lock and key colloids. *Nature* **464**, 575–578 (2010).

[9] Meng, G., Arkus, N., Brenner, M. P. & Manoharan, V. N. The free-energy landscape of clusters of attractive hard spheres. *Science* **327**, 560–563 (2010).

[10] Kraft, D. J. *et al.* Surface roughness directed self-

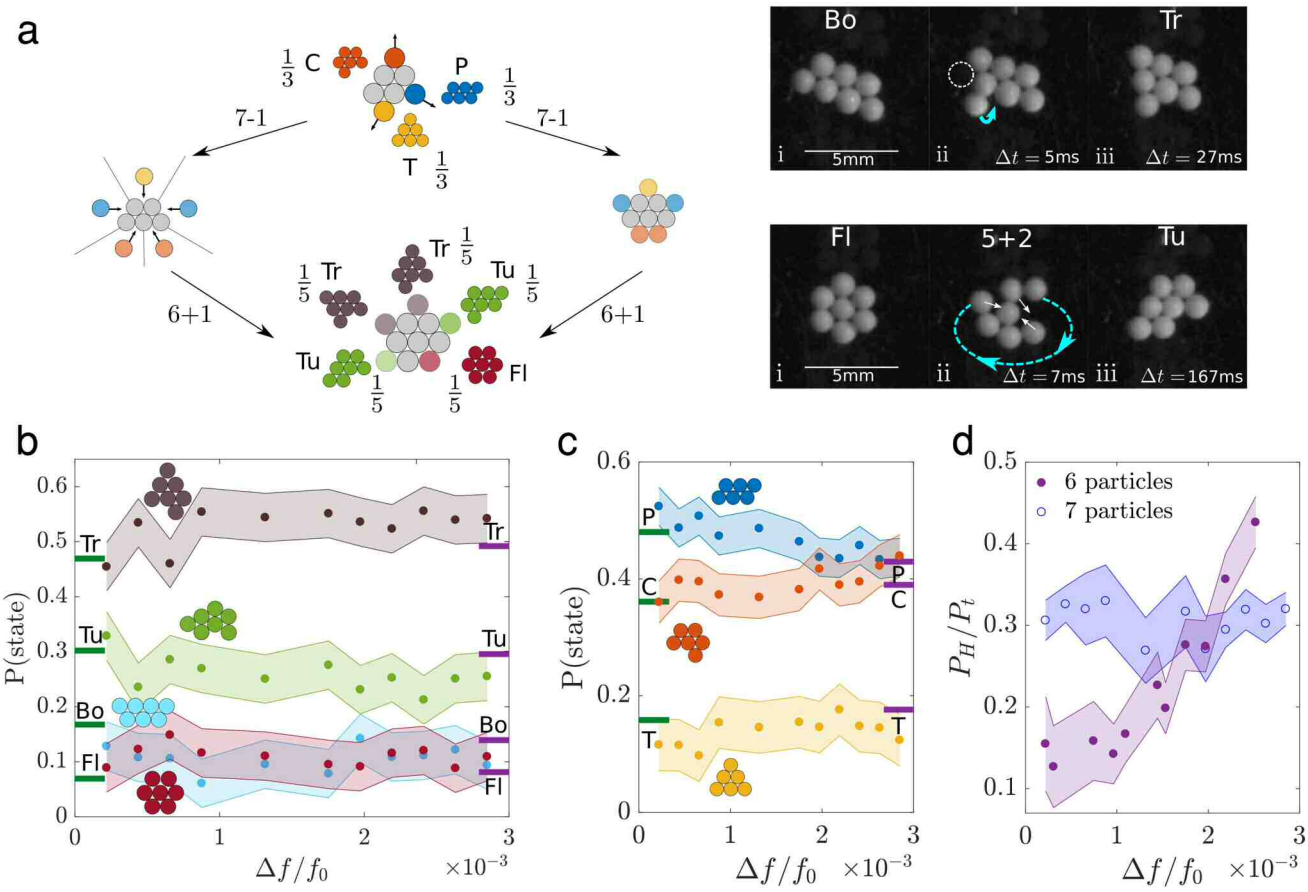

FIG. 4. **Seven-particle cluster assembly, ground-state statistics, and transition states.** (a) Left: Schematic of model for statistics of six- and seven-particle clusters in the acoustic trap. Acoustic frequency tunes the formation of six-particle clusters from sticky (centre left) to ergodic (centre right) regimes. Six-particle clusters can be formed when a particle is removed from the edge of a seven-particle cluster (top). In the reverse process, seven-particle clusters are formed ergodically from six-particle clusters (bottom). Right: Sequence of images from below showing a transition between seven-particle states via a hinge motion (top) or a particle ejection (bottom). See Supplementary Movies 3 and 4 for dynamics. (b) Distribution of seven-particle cluster configurations as a function of detuning parameter, with standard error indicated by shaded area. The green (purple) bars indicate statistics derived from taking into account the sticky (ergodic) six-particle clusters. (c) Statistics of intermediate six-particle clusters within a seven-particle system, plotted as a function of detuning parameter (standard error indicated by shaded area). The green (purple) bars indicate statistics derived from considering sticky (ergodic) cluster assembly. (d) Probability of observing a hinge motion P_H as a fraction of the total number of transitions P_t for different values of the detuning parameter. Filled, purple (hollow, blue) disks correspond to clusters of 6 (7) particles. See Supplementary Information for the number of observations in this data.

assembly of patchy particles into colloidal micelles. *Proceedings of the National Academy of Sciences* **109**, 10787–10792 (2012).

[11] Gorkov, L. P. Forces acting on a small particle in an acoustic field within an ideal fluid. *Sov. Phys. Doklady* **6**, 773–775 (1962).

[12] Wang, M. *et al.* Sound-mediated stable configurations for polystyrene particles. *Phys. Rev. E* **96**, 052604 (2017).

[13] Lee, V., James, N. M., Waitukaitis, S. R. & Jaeger, H. M. Collisional charging of individual submillimeter particles: Using ultrasonic levitation to initiate and track charge transfer. *Physical Review Materials* **2**, 035602 (2018).

[14] Settnes, M. & Bruus, H. Forces acting on a small particle in an acoustical field in a viscous fluid. *Physical Review E* **85**, 016327 (2012).

[15] Rudnick, J. & Barmatz, M. Oscillational instabilities in single-mode acoustic levitators. *The Journal of the Acoustical Society of America* **87**, 81–92 (1990).

[16] Perry, R. W., Holmes-Cerfon, M. C., Brenner, M. P. & Manoharan, V. N. Two-dimensional clusters of colloidal spheres: Ground states, excited states, and structural rearrangements. *Physical Review Letters* **114**, 228301 (2015).

[17] Silva, G. T. & Bruus, H. Acoustic interaction forces between small particles in an ideal fluid. *Physical Review E* **90**, 063007 (2014).

[18] Asakura, S. & Oosawa, F. On interaction between two bodies immersed in a solution of macromolecules. *The Journal of Chemical Physics* **22**, 1255–1256 (1954).

[19] Kudrolli, A., Wolpert, M. & Gollub, J. P. Cluster formation due to collisions in granular material. *Physical Review Letters* **78**, 1383–1386 (1997).

[20] Goldhirsch, I. & Zanetti, G. Clustering instability in dissipative gases. *Physical Review Letters* **70**, 1619–1622 (1993).

[21] Brilliantov, N., Saluena, C., Schwager, T. & Pöschel, T. Transient structures in a granular gas. *Physical Review Letters* **93**, 134301 (2004).

[22] Royer, J. R. *et al.* High-speed tracking of rupture and clustering in freely falling granular streams. *Nature* **459**, 1110–1113 (2009).

[23] Lee, V., Waitukaitis, S. R., Miskin, M. Z. & Jaeger, H. M. Direct observation of particle interactions and clustering in charged granular streams. *Nature Physics* **11**, 733–737 (2015).

[24] Lumay, G. & Vandewalle, N. Controlled flow of smart powders. *Physical Review E* **78**, 061302 (2008).

[25] Fushimi, T., Hill, T. L., Marzo, A. & Drinkwater, B. W. Nonlinear trapping stiffness of mid-air single-axis acoustic levitators. *Applied Physics Letters* **113**, 034102 (2018).

[26] Zhang, S. *et al.* Acoustically mediated long-range interaction among multiple spherical particles exposed to a plane standing wave. *New Journal of Physics* **18**, 113034 (2016).

[27] Glynne-Jones, P., Mishra, P. P., Boltryk, R. J. & Hill, M. Efficient finite element modeling of radiation forces on elastic particles of arbitrary size and geometry. *The Journal of the Acoustical Society of America* **133**, 1885–1893 (2013).

[28] Jambon-Puillet, E., Josserand, C. & Protière, S. Wrinkles, folds, and plasticity in granular rafts. *Physical Review Materials* **1**, 042601 (2017).

[29] Owens, C. E., Shields, C. W., Cruz, D. F., Charbonneau, P. & López, G. P. Highly parallel acoustic assembly of microparticles into well-ordered colloidal crystallites. *Soft Matter* **12**, 717–728 (2016).

[30] Chen, Q., Bae, S. C. & Granick, S. Directed self-assembly of a colloidal kagome lattice. *Nature* **469**, 381–384 (2011).

[31] van Anders, G., Ahmed, N. K., Smith, R., Engel, M. & Glotzer, S. C. Entropically patchy particles: engineering valence through shape entropy. *ACS Nano* **8**, 931–940 (2013).

[32] Cavallaro, M., Botto, L., Lewandowski, E. P., Wang, M. & Stebe, K. J. Curvature-driven capillary migration and assembly of rod-like particles. *Proceedings of the National Academy of Sciences* **108**, 20923–20928 (2011).

Methods

Experiment and Data Analysis. We used a commercial transducer (Hesentec Rank E) to generate ultrasound. An aluminium horn was bolted onto the transducer to maximise the strength of the nodes in the pressure field, following the finite-element optimisation reported in Ref. [S1]. The base of the horn (diameter 38.1mm) was painted black to better image the particles from below. The transducer was driven by applying an AC peak-to-peak voltage of 180V, produced by a function generator (BK Precision 4052) connected to a high-voltage amplifier (A-301 HV amplifier, AA Lab Systems). Objects can be levitated stably for a range of drive amplitudes applied to the transducer. In our setup, the amplitude can be varied from 100 to 400V. The acrylic reflector was mounted on a lab jack and adjusted to a transducer-reflector distance λ_0, corresponding to $f_0 = 45.65$kHz. We note that f_0 depends on the resonant frequency of the ultrasound transducer, and can thus be specified to high accuracy. Stable levitation is possible across a range of a few Hz to either side of the resonant frequency. The acoustic trap was detuned by adjusting the frequency f of the function generator. This detuning is sensitive to changes of order 10Hz for the setup that we use. Across the range of detuning shown in the main text, the object always returns to the nodal plane after a collision with the reflector plate. For detuning larger than 150 Hz or so, the object can no longer be levitated.

As particles we used polyethylene spheres (Cospheric, material density $\rho = 1,000$ kg m^{-3}, diameter $d = 710 - 850\,\mu$m). The particles were stored and all experiments were performed in a humidity- and temperature-controlled environment (40-50% relative humidity, 22-24° C). The acrylic reflector was cleaned with compressed air, ethanol and de-ionised water before each experiment. We neutralised any charges that remained on the reflector with an anti-static device (Zerostat 3, Milty).

For each experimental run six or seven particles were inserted into the trap using a pair of tweezers. Although clusters can be levitated in either the upper or lower of the two nodes shown in Fig. 1b of the main text, due to gravity, particles in the upper node are more easily ejected to the lower node than the other way around. Stable levitation in the lower node is therefore easier than in the upper. If clusters were levitated in the upper node, note that they would collide with the transducer rather than the reflector surface. Video was recorded using a high speed camera (Phantom v12) at 1,000 frames per second.

In order to extract cluster shape information from the raw videos, we thresholded the images, then computed properties of the largest connected region in the resulting image using black-and-white image operations (`regionprops`). These functions are available in Matlab. Since each cluster is associated with a specific set of shape parameters, we computed the number of times a cluster shape was formed, divided by the total number of times that any cluster shape was formed, to obtain the cluster statistics in Figs. 2 and 4 of the main text. Hinge motions were similarly obtained (Fig. 4 of main text). Tables listing the total number of 6-cluster states (7-cluster states) observed for each value of detuning parameter can be found in the Supplementary Information.

We calculated the second moment J of the vertical coordinate z by integrating the distance to the z geometric center of the cluster over the area of the cluster. That is,

$$J = \iint_A (z - z_0)^2 \, dA \,,$$

where z_0 is the z geometric center of the cluster. Note that we define J for the specific 2D projection of the cluster sideview. J is then computed similarly to the cluster topologies and hinge modes from the raw data.

Acoustic Force Modeling. We used finite element modeling software (COMSOL) to model the secondary acoustic force due to scattering between a pair of particles levitated in the acoustic field (Fig. 1e of the main text), using two different methods. A schematic is shown in SI Fig. S2. In both cases, we established a one-dimensional background standing pressure wave with given amplitude, such that the total pressure field $P_{\rm tot}$ is given by the sum of the background pressure wave and the calculated pressure. Since the background pressure wave is one-dimensional, the primary levitation force acts only in the vertical direction throughout the levitation chamber. A particle with radius $a = 0.1\lambda$ is fixed in the center of the trap. The levitation chamber was constructed to be a cylinder of height $3\lambda_0/2$ and diameter $8\lambda_0$. In one case, labelled "point particle" in Fig. 1e of the main text, we computed the force on a point particle in the resulting pressure field by solving the equations for the acoustic field by using the expression derived in Ref. [S2]. In the second case, labelled "fluid-structure interaction" in Fig. 1e of the main text, we computed the force on a second particle of radius $r = 0.1\lambda$ by computing the full fluid-structure interaction, following the method of Ref. [S3].

Note that the calculations shown in Fig. 1e do not account for the finite size of the transducer, which would produce an in-plane potential gradient. In the Supplementary Information, we have done additional calculations that account for the finite size of the transducer. These calculations create a standing wave within the geometry of the trap by applying a driving at fixed frequency to the transducer. We present these results in SI section S2 and Fig. S4, and show that the lateral force from the finite size of the trap is very small in the region of interest near the center of the transducer.

Markov-Chain Model. We consider a discrete-time Markov chain that relates the cluster statistics for five-, six-, and seven-particle clusters by examining the physical processes that produce different clusters. We consider the following mechanisms: (1) Seven particle clusters are formed by ergodically adding a particle to a six-particle cluster (meaning that the particle occupies any binding

site with equal probability). (2) Six-particle clusters are formed from five-particle clusters, in a way that depends on the detuning parameter. (3) Six-particle clusters are also formed from the removal of a particle from the edge of a seven-particle cluster. (4) Five-particle clusters are formed from the removal of a particle from the edge of a six-particle cluster. Denoting the probability of state S as $P(S)$, we write

$$\mathbf{P_7} = \begin{pmatrix} P(Fl) \\ P(Tu) \\ P(Tr) \\ P(Bo) \end{pmatrix}, \mathbf{P_6} = \begin{pmatrix} P(P) \\ P(C) \\ P(T) \end{pmatrix}, \mathbf{P_5} = \begin{pmatrix} P(5) \end{pmatrix} .$$

We recall that there are four possible states for seven-particle clusters, three for six-particle clusters, and one for five-particle clusters. Let $\mathrm{T}_N^{e,s}$ denote the creation matrix that describes building a N-cluster from an $(N-1)$-cluster for either ergodic or sticky processes, and Q_N the destruction matrix for breaking an $N+1$-cluster to make a N-cluster. Then

$$\mathbf{P_7} = \mathrm{T}_7^e \mathbf{P_6}, \tag{S1}$$

$$\mathbf{P_6} = \frac{1}{2}\mathrm{Q}_6 \mathbf{P_7} + \frac{1}{2}\mathrm{T}_6^{e,s} \mathbf{P_5}, \tag{S2}$$

$$\mathbf{P_5} = \mathrm{Q}_5 \mathbf{P_6}. \tag{S3}$$

Note that we assign equal weight to the processes which form a six-particle cluster from a five-cluster, and those which form a six- cluster from a seven-cluster. In addition, T_6 describes either ergodic or sticky six-particle formation processes depending on the detuning parameter.

Six particle statistics

If we exclude the seven-particle processes from the model, we are left with

$$\mathbf{P_6} = \mathrm{T}_6^{e,s} \mathbf{P_5}, \tag{S4}$$

$$\mathbf{P_5} = \mathrm{Q}_5 \mathbf{P_6}. \tag{S5}$$

We construct an effective transition matrix R_{66}, describing the six- to six-cluster transitions through intermediate five-cluster states. Substituting Eq. (S5) into Eq. (S4),

$$\mathrm{R}_{66} = \mathrm{T}_6^{e,s} \mathrm{Q}_5. \tag{S6}$$

To find Q_5, we consider the possible clusters that result from removing a particle from the edge of a cluster. Trivially, removing any particle from a six-cluster results in the unique five-cluster:

$$\mathrm{Q}_5 = \begin{pmatrix} 1 & 1 & 1 \end{pmatrix}. \tag{S7}$$

In addition, $\mathrm{T}_6^{e,s}$ are constructed from the ergodic and sticky models:

$$\mathrm{T}_6^e = \begin{pmatrix} 2/5 \\ 2/5 \\ 1/5 \end{pmatrix}, \mathrm{T}_6^s = \begin{pmatrix} 1/2 \\ 1/3 \\ 1/6 \end{pmatrix}. \tag{S8}$$

Since the steady state probability vector $\mathbf{P_6}$ satisfies $\mathbf{P_6} = R_{66}\mathbf{P_6}$, we find $\mathbf{P_6}$ by finding the eigenvector of R_{66} with unit eigenvalue. Substituting

$$\mathbf{P_6^e} = \begin{pmatrix} 2/5 \\ 2/5 \\ 1/5 \end{pmatrix}, \mathbf{P_6^s} = \begin{pmatrix} 1/2 \\ 1/3 \\ 1/6 \end{pmatrix} .$$

These probabilities are shown in Fig. 2b of the main text.

Seven particle statistics

Similarly to the six-cluster derivation, we derive expressions for the effective transition matrices M_{77} and M_{66} from Eqs. (S1)-(S3), such that $\mathbf{P_7} = \mathrm{M}_{77}\mathbf{P_7}$ and $\mathbf{P_6} = \mathrm{M}_{66}\mathbf{P_6}$. The steady-state probabilities are then the eigenvectors of M_{66} and M_{77} with unit eigenvalue. Note that M_{77} and M_{66} include transitions through five- and six-cluster intermediates. Substituting Eqs. (S1) and (S3) into (S2), we obtain

$$M_{66} = \frac{1}{2}\mathrm{Q}_6\mathrm{T}_7^e + \frac{1}{2}\mathrm{T}_6^{e,s}\mathrm{Q}_5 \,. \tag{S9}$$

We derive M_{77} by substituting Eq. (S3) into (S2), which is then substituted for $\mathbf{P_6}$ in Eq. (S1):

$$\begin{aligned} \mathbf{P_7} &= \mathrm{T}_7^e \left(\frac{1}{2}\mathrm{Q}_6 \mathbf{P_7} + \frac{1}{2}\mathrm{T}_6^{e,s}\mathrm{Q}_5 \mathbf{P_6} \right) \\ &= \frac{1}{2}\mathrm{T}_7^e\mathrm{Q}_6\mathbf{P_7} + \frac{1}{2}\mathrm{T}_7^e\mathrm{T}_6^{e,s}\mathrm{Q}_5\mathbf{P_6} \end{aligned}$$

In order to get a closed-form expression for $\mathbf{P_7}$, we continue substituting for P_6:

$$\begin{aligned} \mathbf{P_7} &= \frac{1}{2}\mathrm{T}_7^e\mathrm{Q}_6\mathbf{P_7} + \frac{1}{2}\mathrm{T}_7^e\mathrm{T}_6^{e,s}\mathrm{Q}_5 \left(\frac{1}{2}\mathrm{Q}_6\mathbf{P_7} + \frac{1}{2}\mathrm{T}_6^{e,s}\mathrm{Q}_5\mathbf{P_6} \right) \\ &= \frac{1}{2}\mathrm{T}_7^e\mathrm{Q}_6\mathbf{P_7} + \frac{1}{4}\mathrm{T}_7^e\mathrm{T}_6^{e,s}\mathrm{Q}_5\mathrm{Q}_6\mathbf{P_7} \\ &+ \frac{1}{4}\mathrm{T}_7^e\mathrm{T}_6^{e,s}\mathrm{Q}_5\mathrm{T}_6^{e,s}\mathrm{Q}_5\mathbf{P_6} \end{aligned}$$

This leads to a geometric series in increasing numbers of transitions between five- and six-cluster states:

$$\mathbf{P_7} = \frac{1}{2}\mathrm{T}_7^e\mathrm{Q}_6\mathbf{P_7} + \left(\sum_{n=1}^{\infty} \frac{1}{2^{n+1}} \mathrm{T}_7^e (\mathrm{T}_6^{e,s}\mathrm{Q}_5)^n \mathrm{Q}_6 \right) \mathbf{P_7}$$

We note that $\mathrm{T}_6^{e,s}\mathrm{Q}_5$ is idempotent, so that $(\mathrm{T}_6^{e,s}\mathrm{Q}_5)^n = \mathrm{T}_6^{e,s}\mathrm{Q}_5$ for any n. Then we complete the geometric series and write

$$M_{77} = \frac{1}{2}\mathrm{T}_7^e\mathrm{Q}_6 + \frac{1}{2}\mathrm{T}_7^e\mathrm{T}_6^{e,s}\mathrm{Q}_5\mathrm{Q}_6 \tag{S10}$$

To find the destruction matrix Q_6, we assume that any particle on the edge of a cluster has equal probability to be removed. Then Fl can only make C, Tu makes P and C with equal probability, Tr makes P, C, and T equally, and Bo makes only P:

$$\mathrm{Q}_6 = \begin{pmatrix} 0 & 1/3 & 1/2 & 1 \\ 1 & 1/3 & 1/2 & 0 \\ 0 & 1/3 & 0 & 0 \end{pmatrix}$$

Similarly, we construct T_7^e assuming that a seventh particle has equal probability to attach to any binding site on a six-particle cluster:

$$\mathrm{T}_7^e = \begin{pmatrix} 0 & 1/5 & 0 \\ 1/3 & 2/5 & 1 \\ 1/3 & 2/5 & 0 \\ 1/3 & 0 & 0 \end{pmatrix}$$

Substituting into Eqs. S9 and S10 and solving the eigenvalue problem, as for the six-particle clusters, gives

$$\mathbf{P_7^s} = \begin{pmatrix} 0.071 \\ 0.464 \\ 0.303 \\ 0.161 \end{pmatrix}, \mathbf{P_7^e} = \begin{pmatrix} 0.079 \\ 0.480 \\ 0.299 \\ 0.141 \end{pmatrix}$$

and

$$\mathbf{P_6^s} = \begin{pmatrix} 0.484 \\ 0.355 \\ 0.161 \end{pmatrix}, \mathbf{P_6^e} = \begin{pmatrix} 0.426 \\ 0.349 \\ 0.180 \end{pmatrix}$$

The data that support the plots within this paper and other findings of this study are available from the corresponding author upon request.

[S1] Andrade, M. A. B., Buiochi, F. & Adamowski, J. C. Finite element analysis and optimization of a single-axis acoustic levitator. *IEEE Transactions on Ultrasonics, Ferroelectrics, and Frequency Control* **57**, 469–479 (2010).

[S2] Gorkov, L. P. Forces acting on a small particle in an acoustic field within an ideal fluid. *Sov. Phys. Doklady* **6**, 773–775 (1962).

[S3] Glynne-Jones, P., Mishra, P. P., Boltryk, R. J. & Hill, M. Efficient finite element modeling of radiation forces on elastic particles of arbitrary size and geometry. *The Journal of the Acoustical Society of America* **133**, 1885–1893 (2013).

Cluster formation by acoustic forces and active fluctuations in levitated granular matter: Supplementary Information

Melody X. Lim,[1,2] Anton Souslov,[1,3] Vincenzo Vitelli,[1,2] and Heinrich M. Jaeger[1,2]

[1] *James Franck Institute, The University of Chicago, Chicago, Illinois 60637, USA*

[2] *Department of Physics, The University of Chicago, Chicago, Illinois 60637, USA*

[3] *Department of Physics, University of Bath, Bath BA2 7AY, United Kingdom*

S1. THERMAL SEVEN-PARTICLE CLUSTERS

For thermal clusters, the flower is the only ground state of the seven-particle system, since it has one more bond than the tree, turtle, or boat. For this reason, in a thermal system, the relative occupation probabilities of the four possible configurations are a function of the temperature. These statistics can be calculated as follows.

Let the energy of each bond be E_B. Then we define the flower as having zero energy (the only ground state), and the tree, turtle, and boat as being at energy E_B each. Then the partition function of the system is

$$\begin{aligned} Z &= \sum_i \mathrm{e}^{-E_i/k_BT} \\ &= n_{Fl} + (n_{Tr} + n_{Tu} + n_{Bo})\mathrm{e}^{-E_B/k_BT} \end{aligned}$$

where n_i is the degeneracy of each possible cluster configuration, T is the temperature, and k_B is the Boltzmann factor. To determine the degeneracy of each cluster configuration, we count the number of ways to make a given configuration from a six-particle cluster, multiplied by the degeneracy of that six-particle cluster. The flower can be made only one way (add a particle to the chevron), but the chevron can be made two ways from the five-particle cluster, so $n_{Fl} = 2$. Similarly, the boat can be made two ways from the parallelogram, and the parallelogram two ways from the five-particle cluster, so $n_{Bo} = 4$. The turtle can be made two ways from the parallelogram, and two from the chevron, so $n_{Tu} = 8$. Finally, the tree can be made in two ways from the parallelogram, two ways from the chevron, and six from the triangle (which can only be made one way from the five-particle cluster), so that $n_{Tr} = 14$. The probability of each state as a function of temperature is thus:

$$\begin{aligned} \mathrm{P(Fl)} &= \frac{2}{2 + 14\mathrm{e}^{-E_B/k_BT}} \\ \mathrm{P(Bo)} &= \frac{4}{2\mathrm{e}^{E_B/k_BT} + 14} \\ \mathrm{P(Tu)} &= \frac{8}{2\mathrm{e}^{E_B/k_BT} + 14} \\ \mathrm{P(Tr)} &= \frac{14}{2\mathrm{e}^{E_B/k_BT} + 14} \end{aligned}$$

These probabilities are plotted as a function of k_BT/E_B in Fig. S1. For reference, the probabilities from the Markov-chain model used in the main text are also shown. Within error of our experiment, the Markov-chain predictions in the ergodic regime are indistinguishable from the high-temperature limit of the thermal seven-particle clusters ($k_BT > 2E_B$). Thus the failure of the system to find the global ground state even in the ergodic limit suggests that our large detuning limit is most analogous to a high temperature thermal system.

S2. ACOUSTIC FORCES AND THE CONFINING POTENTIAL

In order to compare the relative importance of the primary and secondary radiation forces, we carry out a second set of calculations that take into account the finite size of the acoustic trap. By primary forces, we mean the lateral components of the acoustic force on a single particle within the nodal plane, which arise from the finite size of the acoustic trap. Secondary forces refer to the interaction forces induced by the presence of a second particle in the acoustic field. Figure S4 shows simulations in which we mimic the experimental conditions by applying a normal acceleration at fixed frequency and amplitude to the top boundary of a trap, while enforcing a perfectly reflecting bottom boundary. At the same time, we impose plane wave radiation conditions on the right hand boundary of the trap, such that the finite size of the transducer produces a lateral force towards the center of the acoustic trap. These boundary conditions are different to the ones that were used to produce the results in Fig. 1e of the main text and in Fig S2, in which a one-dimensional standing wave was established as a background pressure field, but without the open radiation conditions at the edge of the transducer. Note that the results in Fig. 1e correspond to the difference between the secondary and primary radiation forces calculated here (since the results in Fig. 1e correspond to calculating only the secondary forces, without regard to the primary forces).

We compare the in-plane acoustic force F_A on a point particle for two cases: (1) the point particle subject only to a standing wave, accounting for the finite size of the transducer as described above (primary force), and (2) the point particle with a perfectly scattering particle fixed in the center of the trap (primary and secondary). Simulation results are shown in Fig. S4b. When the test particle is far from the trap center ($r \gtrsim 2\lambda$), the difference between cases (1) and (2) is small, indicating that the primary radiation force dominates for a particle far from the trap center. In contrast, when the test particle is close to the trap center (the regime relevant to the experiments, where the particles form clusters in which they effectively 'bond'), the secondary force is larger than the primary by 2 orders of magnitude.

SUPPLEMENTARY FIGURES

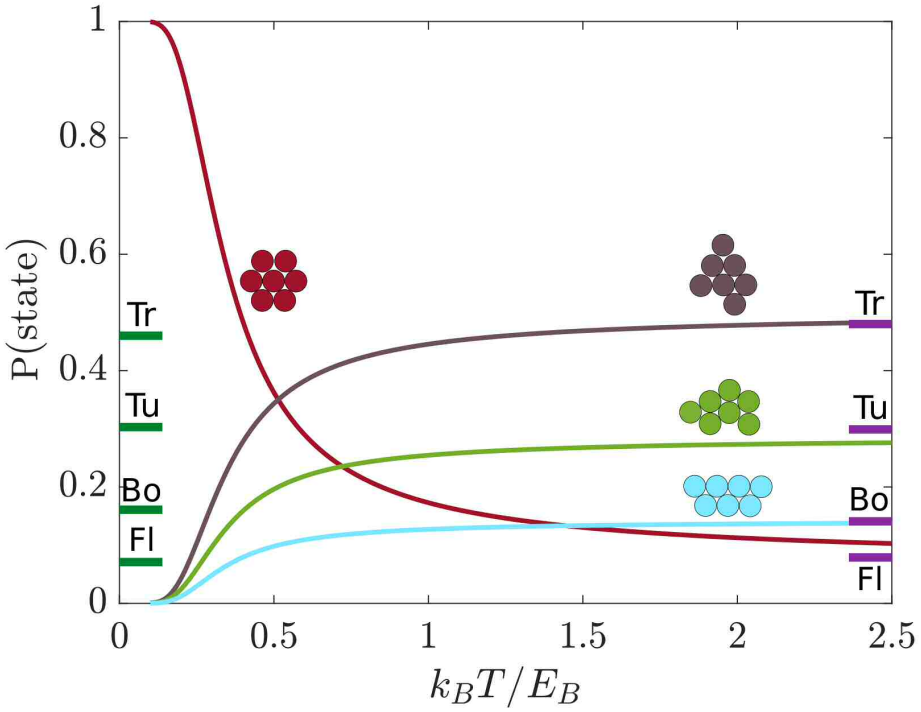

FIG. S1. **Predicted statistics for thermal seven-particle clusters.** Cluster statistics for thermal seven-particle clusters as a function of k_BT/E_B (solid curves). See section S1 for derivation. The probabilities from the Markov-chain model in the ergodic (sticky) regime used in the main text are also shown as purple (green) bars. Within error of our experiment, the Markov-chain predictions in the ergodic regime are indistinguishable from the high-temperature limit of the thermal seven-particle clusters ($k_BT > 2E_B$).

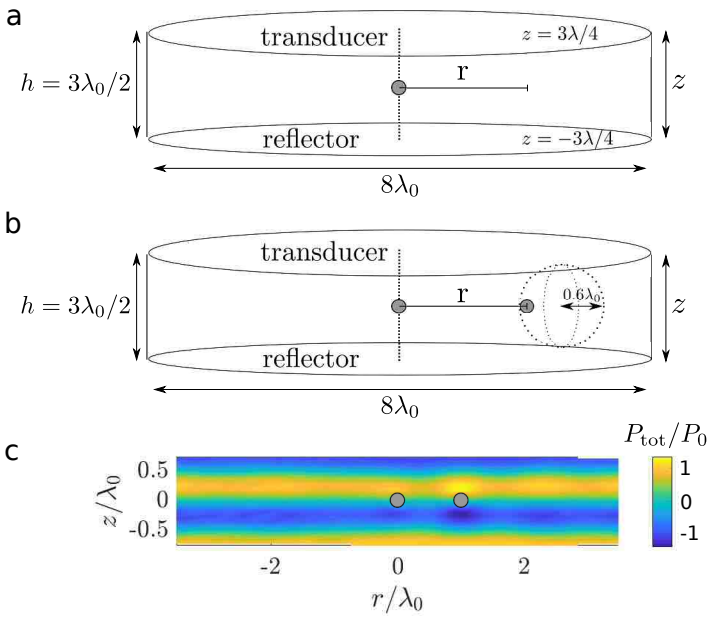

FIG. S2. **Finite element model for acoustic forces.** We used finite element modeling software (COMSOL) to model the force between a pair of particles levitated in the three-dimensional acoustic field, using two different methods. In both cases, we established a background standing pressure wave in the vertical direction with given amplitude P_0, such that the background pressure is $P_{\mathrm{b}}(z) = P_0 \sin(2\pi z/\lambda)$. A perfectly reflecting particle (radius $a = 0.1\lambda$) is fixed in the center of the trap. The levitation chamber was constructed to be a cylinder of height $3\lambda_0/2$ and width $8\lambda_0$. The pressure boundary conditions on the surface of the cylinder match the background pressure condition $P(z)$. These boundary conditions do not include the free radiation conditions along the side wall of the cylinder, which induce an additional horizontal force, which, however, is negligible in the region of interest (see Fig. S4). Note that these diagrams are to scale. (a) In one case, labelled "point particle" in Fig. 1e of the main text, we computed the force on a point particle in the resulting 3D pressure field by solving the equations for the acoustic field, using the expression derived in Ref. [1]. This gives an acoustic potential, the gradient of which then gives the acoustic force on a point particle at distance r from the center of the trap. (b) In the second case, labelled "fluid-structure interaction" in Fig. 1e of the main text, we computed the force on a second particle of radius $a = 0.1\lambda$, which can deform elastically, by computing the full fluid-structure interaction following the method of Ref. [2]. The force on the second particle is computed by integrating the momentum flux over an integration surface, which is a sphere with radius 0.6λ (dotted lines). The sphere is placed so as not to intersect the particles. (c) Total pressure $P_{\mathrm{tot}} = P + P_{\mathrm{b}}$, normalised by P_0. Results were computed using fluid-structure interaction, for particle spacing $x = \lambda_0$. Grey circles indicate the position of the particles.

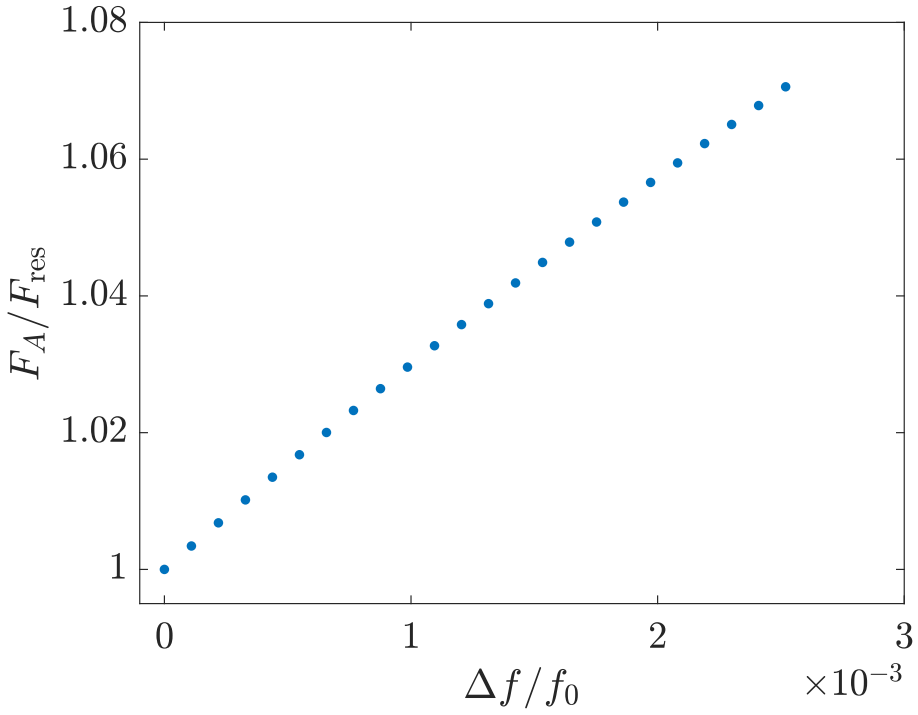

FIG. S3. **Secondary acoustic force as a function of detuning parameter.** We used finite element modelling, as in Fig. S2 and Fig. 1e of the main text, to determine the variation of the secondary acoustic force due to scattering F_A between a pair of particles as a function of detuning parameter $\Delta f/f_0$ (not including in-plane contributions from the primary radiation force due to the finite size of the transducer, see Fig. S4). For this calculation, $r = 0.25\lambda$, and all geometrical parameters are fixed in terms of λ_0 while the wavelength of the standing wave is detuned. We plot F_A normalised by the force at resonance, F_{res}. The magnitude of acoustic force increases less than 10% for the experimental range of detuning.

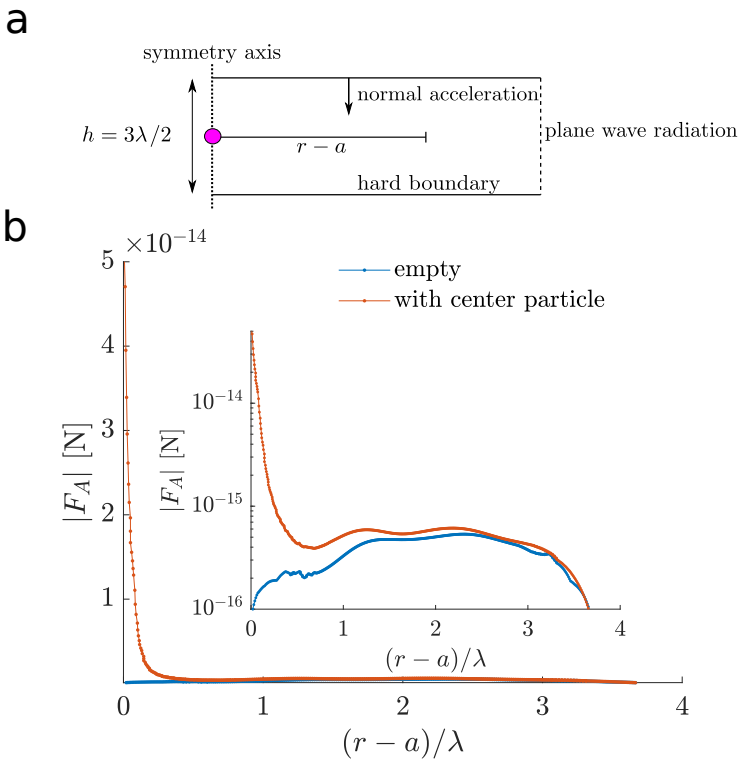

FIG. S4. **Secondary acoustic forces dominate dynamics in the levitation plane.** (a) Simulation geometry. The axisymmetric acoustic cavity (symmetry axis as labelled above) is modeled using a finite-element simulation. The top of the cavity is driven at a fixed normal acceleration and frequency (0.1m/s^2 and 45.651kHz for the results shown here), while the bottom enforces a sound hard boundary (perfectly reflecting) condition. We apply a plane-wave radiation condition to the right boundary (dashed line) to mimic the finite size of the transducer in the experiment. Note that these are different boundary conditions to those used to compute the results in Fig. 1e of the main text (compare these schematics to Fig. S2). The lateral acoustic force F_A as a function of r, the distance from the center, on a point scatterer in the levitation plane is calculated from the resulting pressure and velocity field according to the expression derived in Ref. [1]. F_A is calculated for two different configurations: (1) the point scatterer subject only to a standing wave ("empty"), or (2) a perfectly scattering particle of radius $a = 0.1\lambda$ fixed in the center of the trap ("with center particle"). (b) Comparison of the force on a point scatterer due purely to the trap (blue, primary force), to the force on a point scatterer due to the presence of another particle (red, combined primary and secondary forces or acoustic force). Inset: same as main figure, with a log-scale y-axis. When the particles are close, the secondary acoustic force can be larger than the radial force due to the primary confining potential by 2 orders of magnitude.

SUPPLEMENTARY TABLES

$\Delta f/f_0 \times 10^{-3}$	number of observations
0.31	347
0.74	360
0.96	639
1.10	665
1.45	472
1.53	1305
1.75	1992
1.97	1393
2.19	2114
2.52	584

TABLE S1. Number of observations for 6-clusters

$\Delta f/f_0 \times 10^{-3}$	number of observations
0.22	843
0.44	1151
0.66	350
0.88	1103
1.32	671
1.75	1136
1.97	1329
2.19	1869
2.41	1454
2.63	1372
2.85	1537

TABLE S2. Number of observations for 7-clusters

DESCRIPTION OF SUPPLEMENTARY MOVIES

Supplementary Movie 1: Topological reconfigurations of six-particle clusters. Part 1: Bottom view of a six-particle cluster levitated in an acoustic field, which is close to its resonant frequency ($\Delta f/f_0 = 0.25 \times 10^{-3}$). The cluster rearranges between its three distinct ground states. Playback is slowed down by a factor of 10. The real-time duration of the movie is 3.5 seconds. Bottom view of a six-particle cluster levitated in an acoustic field, which is driven far from its resonant frequency ($\Delta f/f_0 = 2.5 \times 10^{-3}$). The cluster rearranges between its three distinct ground states. Playback is slowed down by a factor of 10. The real-time duration of the movie is 1.8 seconds.

Supplementary Movie 2: Out-of-plane cluster fluctuations. Part 1: Side view of a six-particle cluster levitated in an acoustic field, which is close to its resonant frequency ($\Delta f/f_0 = 0.25 \times 10^{-3}$). The cluster oscillates vertically in the trap, until it strikes the acrylic reflector, breaking the cluster. The cluster remains in a planar configuration before and after the collision. Playback is slowed down by a factor of 10. The real-time duration of the movie is 2 seconds. Part 2: Bottom view of a six-particle cluster levitated in an acoustic field, which is driven far from its resonant frequency ($\Delta f/f_0 = 2.5 \times 10^{-3}$). The cluster oscillates vertically in the trap, exciting out-of-plane bending modes. Playback is slowed down by a factor of 10. The real-time duration of the movie is 0.7 seconds.

Supplementary Movie 3: Cluster rearrangement via particle ejection. Part 1: Bottom view of a six-particle cluster levitated in an acoustic field, which is close to its resonant frequency ($\Delta f/f_0 = 0.25 \times 10^{-3}$). The cluster (initially Parallelogram) rearranges by breaking into a five-particle cluster and a single particle, which then recombine to a different six-particle configuration (Chevron). Playback is slowed down by a factor of 100. The real-time duration of the movie is 1.7 seconds. Part 2: Bottom view of a seven-particle cluster levitated in an acoustic field, which is detuned from its resonant frequency ($\Delta f/f_0 = 1.3 \times 10^{-3}$). The cluster (initially Flower) rearranges by breaking into a five-particle cluster and two single particles, which then recombine to a different seven-particle configuration (Turtle). Playback is slowed down by a factor of 33. The real-time duration of the movie is 0.6 seconds.

Supplementary Movie 4: Cluster rearrangement via hinge motion. Part 1: Bottom view of a six-particle cluster levitated in an acoustic field, which is driven far from its resonant frequency ($\Delta f/f_0 = 2.5 \times 10^{-3}$). The cluster (initially Parallelogram) rearranges

via a hinge motion to a different six-particle configuration (Triangle). Playback is slowed down by a factor of 100. The real time duration of the movie is 9 milliseconds. Part 2: Bottom view of a seven-particle cluster levitated in an acoustic field, which is driven far from its resonant frequency ($\Delta f/f_0 = 2.2 \times 10^{-3}$). The cluster (initially Boat) rearranges via a hinge motion to a different seven-particle configuration (Turtle). Playback is slowed down by a factor of 100. The real-time duration of the movie is 20 milliseconds.

---

[1] Gorkov, L. Forces acting on a small particle in an acoustic field within an ideal fluid. *Sov. Phys. Doklady* **6**, 773–775 (1962).

[2] Glynne-Jones, P., Mishra, P. P., Boltryk, R. J. & Hill, M. Efficient finite element modeling of radiation forces on elastic particles of arbitrary size and geometry. *The Journal of the Acoustical Society of America* **133**, 1885–1893 (2013).